JCN RESEARCH IN SYSTEMS NEUROSCIENCE THE JOURNAL OF COMPARATIVE NEUROLOGY WILEY

Female reproductive state is associated with changes in distinct arginine vasotocin cell types in the preoptic area of *Astatotilapia burtoni*

Julie M. Butler [ORCID] | Chase M. Anselmo | Karen P. Maruska [ORCID]

Department of Biological Sciences, Louisiana State University, Baton Rouge, Louisiana

Correspondence
Julie M. Butler, Department of Biology, Stanford University, 371 Jane Stanford Way, Gilbert 304, Stanford, CA, 94305-5020.
Email: jmbutler@stanford.edu

Abstract

Nonapeptides play a crucial role in mediating reproduction, aggression, and parental care across taxa. In fishes, *arginine vasotocin* (AVT) expression is related to social and/or reproductive status in most male fishes studied to date, and is linked to territorial defense, paternal care, and courtship. Despite a plethora of studies examining AVT in male fishes, relatively little is known about how AVT expression varies with female reproductive state or its role in female social behaviors. We used multiple methods for examining the AVT system in female African cichlid fish *Astatotilapia burtoni*, including immunohistochemistry for AVT, in situ hybridization for *avt*-mRNA, and quantitative PCR. Ovulated and mouthbrooding females had similar numbers of parvocellular, magnocellular, and gigantocellular AVT cells in the preoptic area. However, ovulated females had larger magnocellular and gigantocellular cells compared to mouthbrooding females, and gigantocellular AVT cell size correlated with the number of days brooding, such that late-stage brooding females had larger AVT cells than mid-stage brooding females. In addition, we found that ventral hypothalamic cells were more prominent in females compared to males, and were larger in mouthbrooding compared to ovulated females, suggesting a role in maternal care. Together, these data indicate that AVT neurons change across the reproductive cycle in female fishes, similar to that seen in males. These data on females complement studies in male *A. burtoni*, providing a comprehensive picture of the regulation and potential function of different AVT cell types in reproduction and social behaviors in both sexes.

Abbreviations: ATn, anterior tuberal nucleus; CP, central posterior thalamic nucleus; DP, dorsal posterior thalamic nucleus; Dd, dorsal part of dorsal telencephalon; Dl, lateral part of dorsal telencephalon; Dm, medial part of dorsal telencephalon; Gn, glomerular nucleus; h, habenula; LL, lateral lemniscus; mlf, medial longitudinal fasciculus; nGMp, magnocellular preoptic nucleus, gigantocellular division; NLT, lateral tuberal nucleus; NLTv, ventral subdivision of NLT; nMMp, magnocellular preoptic nucleus, magnocellular division; nPMp, parvocellular preoptic nucleus, gigantocellular division; nPPa, parvocellular preoptic nucleus, anterior part; nPPp, parvocellular preoptic nucleus, posterior part; NRL, nucleus of the lateral recess; ON, optic nerve; PGa, anterior preglomerular nucleus; PGc, commissural preglomerular nucleus; PHT, preoptico-hypophyseal tract; Pit, pituitary; POA, preoptic area; sgt, secondary gustatory tract; T, tectum; TBT, tectobulbar tract; TPp, periventricular nucleus of posterior tuberculum; Vc, central part of ventral telencephalon; VCeG, granular zone of the valvula cerebellum; Vd, dorsal part of ventral telencephalon; Vde, descending tract of trigeminal nucleus; Vl, lateral part of ventral telencephalon; Vs, supracommissural part of ventral telencephalon; VTn, ventral tuberal nucleus; Vv, ventral part of ventral telencephalon.

1 | INTRODUCTION

The nonapeptide arginine vasotocin (AVT) is found in all non-mammalian vertebrates, and through a series of ancient gene duplications, gave rise to the present AVT-derived nonapeptide family, including arginine vasopressin (AVP) found in mammals (Acher & Chauvet, 1995). Nonapeptides, including AVT/AVP, are extensively studied for their capacity to modulate complex social behaviors across taxa (e.g., Godwin & Thompson, 2012; Kelly & Goodson, 2014). Because of the broad taxonomic evidence illustrating important conserved functions, examining the distribution and plasticity in the AVT system will provide insights for understanding the evolution of neural circuits involved in context-dependent behaviors.

In fishes, AVT neurons are predominantly found in three different cell populations within the preoptic area (POA; e.g., Dewan, Maruska, & Tricas, 2008; Godwin & Thompson, 2012; Greenwood, Wark, Fernald, & Hofmann, 2008; Kagawa et al., 2016; Maruska, 2009; van den Dungen, Buijs, Pool, & Terlou, 1982). Small parvocellular AVT-immunoreactive (–ir) neurons line the rostroventral POA along the third ventricle (3v) and are thought to be homologous to the tetrapod supraoptic nucleus (Godwin & Thompson, 2012). Magnocellular and gigantocellular AVT-ir neurons lie more caudally and are hypothesized to be homologous to the paraventricular nucleus in tetrapods (Kapsimali, Bourrat, & Vernier, 2001; Olivereau, Moons, Olivereau, & Vandesande, 1988). POA AVT-ir fibers project to the neurohypophysis where AVT is systemically released, but AVT-ir fibers are also found throughout the telencephalon and diencephalon, with the densest AVT-ir fibers often found in the ventral telencephalon (Dewan, Ramey, & Tricas, 2011; Goossens, Dierickx, & Vandesande, 1977; Ohya & Hayashi, 2006; Saito, Komatsuda, & Urano, 2004). In many fishes, an additional group of AVT cells is present in the tuberal region of the ventral hypothalamus (Goodson, Evans, & Bass, 2003; Greenwood et al., 2008; Kagawa et al., 2016; Ohya & Hayashi, 2006).

Despite the reported restricted expression of AVT in the POA and tuberal hypothalamus across all teleosts studied to date (Goodson & Bass, 2000; Kagawa et al., 2016), a recent study suggested *avt* pre-prohormone mRNA (i.e., sequence for *avt* and associated neurophysin) is found throughout the telencephalon of the African cichlid fish *Astatotilapia burtoni* (Rodriguez-Santiago, Nguyen, Winton, Weitekamp, & Hofmann, 2017). However, other studies in the same species have not described this same widespread distribution despite using the same primer sequences for in situ hybridization (ISH) riboprobe generation (Greenwood et al., 2008) (Table 1). These differences are likely due to methodology, but a more detailed and well-controlled study is needed for comparison of AVT immunoreactivity and mRNA distribution in the same species to clarify these previous findings. These discrepancies among studies in the same species also highlight the critical importance of providing staining validation and proper experimental controls to accurately interpret AVT distribution and function.

AVT expression often varies by sex, social/reproductive state, seasonality, and even time of day (Dewan et al., 2008; Dewan et al., 2011; Gozdowska, Kleszczyńska, Sokołowska, & Kulczykowska, 2006; Kagawa, 2013; Ramallo, Grober, Cánepa, Morandini, & Pandolfi, 2012; Rodríguez-Illamola, Patiño, Soengas, Ceinos, & Míguez, 2011). Teleost fishes are a particularly interesting clade for investigating the AVT system because of their diverse reproductive tactics, including sex change, simultaneous hermaphrodism, pair bonding, group/aggregate spawning, mouthbrooding, dominance hierarchies, and harems, among others. While many studies examined the role of nonapeptides, especially AVT, in relation to social behaviors, the vast majority of studies only examined AVT in male fishes (for review, see Godwin & Thompson, 2012). Studies in some fish species, however, did examine AVT neuron differences in both sexes, and across different social or reproductive states including in sex changing fishes (Godwin, Sawby, Warner, Crews, & Grober, 2000; Semsar & Godwin, 2003) and some coral reef species such as butterflyfishes (Dewan et al., 2008; Dewan et al., 2011),

Study	Method	Telen.	POA	NLTv	PGa
Rodriguez-Santiago et al. (2017)	ISH	+	+	n/a	n/a
Greenwood et al. (2008)	ISH	–	+	+	–
Present study	ISH	–	+	+	+
Loveland and Fernald (2017)	IHC	–	+	–	–
Present study	IHC	–	+	–	–

TABLE 1 Expression of AVT cell bodies in *A. burtoni* has diverse reported results. Our results match those previously published *for A. burtoni* by Greenwood et al. (2008) and Loveland and Fernald (2017). In contrast, we found no *avt* preprohormone expression in the telencephalon. Importantly, all three ISH studies used the same primers for probe preparation

Abbreviations: AVT, arginine vasotocin; IHC, immunohistochemistry; ISH, in situ hybridization; NLTv, ventral subdivision of lateral tuberal nucleus; PGa, anterior preglomerular nucleus; POA, preoptic area.

damselfishes (Maruska, 2009), and gobies (Maruska, Mizobe, & Tricas, 2007). These studies suggest a conserved role for AVT in fish reproduction and aggression, but with some variability based on species. While many studies documented the presence or absence of sexually dimorphic AVT expression and immunoreactivity, these studies have largely grouped females into a single category while separating males by reproductive or social status. However, gonadal steroids, especially estradiol help maintain and regulate AVT/AVP levels in the brains of fishes, amphibians, and mammals (Boyd, 1994; Kalamarz-Kubiak, Gozdowska, Guellard, & Kulczykowska, 2017; Miller, Urban, & Dorsa, 1989; Sladek & Somponpun, 2008), suggesting that female reproductive state regulates AVT expression and production. Thus, it is important to examine plasticity of the AVT system in females, as they also undergo cyclical changes in behaviors (aggressive, reproductive, parental) and reproductive physiology comparable to males in many species.

The cichlid fish *A. burtoni* is an excellent model for neuroethology research due to their well-characterized social behaviors (Maruska & Fernald, 2018). Male *A. burtoni* exist on a continuum ranging from dominant to subordinate (Fernald, 1977; Fernald & Hirata, 1977). Dominant males are brightly colored; hold spawning territories that they defend from other males, and actively court gravid and ovulated females for spawning. Subordinate males are drably colored, reproductively repressed, and often associate with females. During spawning, males nip at a female's urogenital opening, stimulating her to release eggs onto the substrate and then pick them up into her buccal cavity. She then nips at the egg spots on the male's anal fin and he releases sperm to fertilize the eggs in her mouth. Females then carry the developing offspring for ~2 weeks, a phase termed mouthbrooding. Mouthbrooding females will aggressively defend a shelter from other females, especially later in the brooding cycle, presumably to provide a safe haven for releasing and protecting their young (Field & Maruska, 2017). In female-only communities, females will also establish a male-like hierarchy dependent on their reproductive state (Renn, Fraser, Aubin-Horth, Trainor, & Hofmann, 2012). As such, investigating differences in the AVT system of females of different reproductive states and comparing this with males displaying similar behaviors provides insights on sex-specific functions.

The AVT system was studied previously in different experimental contexts in *A. burtoni* males (Greenwood et al., 2008; Loveland & Fernald, 2017; Loveland & Hu, 2018; Rodriguez-Santiago et al., 2017). Dominant males have higher *avt*-mRNA expression in the posterior POA (gigantocellular cells) than subordinate males. In the anterior POA (parvocellular cells), subordinate males have higher *avt*-mRNA expression than dominant males (Greenwood et al., 2008). Importantly, gigantocellular *avt*-mRNA expression correlated with the number of aggressive displays while parvocellular *avt*-mRNA expression correlated with submissive behaviors (e.g., fleeing) (Greenwood et al., 2008). In addition, males engaged in aggressive interactions had greater activation of magnocellular POA AVT-ir cells than control males or those engaged in courtship (Loveland & Fernald, 2017). Despite how well studied the AVT system is in males, we know nothing about the AVT system in female *A. burtoni*.

Our primary goal here was to investigate the AVT system in female *A. burtoni*, a species where the male AVT system is extensively studied and in which females undergo similar changes in social behaviors related to the reproductive cycle. We compared cell number (as a proxy for *avt*/AVT production, storage, and/or release) and size (proxy for amount of *avt*/AVT produced/stored per cell) of neurons labeled with AVT antibody or mRNA riboprobe in the brain of ovulated and mouthbrooding females. We also quantified relative *avt* mRNA expression in the POA and two telencephalic regions via quantitative RT-PCR. A secondary goal was to compare the different methodological approaches (immunohistochemistry [IHC], ISH, and qRT-PCR; soma size vs. counts) commonly used across species for measuring AVT abundance/expression, which all yielded differing results, but collectively suggest the AVT system is modulated by female reproductive state. Finally, we aimed to determine if AVT expression in *A. burtoni* is restricted to the POA and ventral hypothalamus or more widespread, as suggested by (Rodriguez-Santiago et al., 2017). Using the same primers as previous studies, but a different ISH protocol and development technique, our distribution matched that classically described for all other teleost fishes and not this more recently reported widespread neural localization. AVT peptide-containing cells were only found in the POA, while *avt* mRNA-containing cells were found in the POA and ventral hypothalamus. No AVT-ir or *avt*-mRNA stained cells were found in the telencephalon. Overall, these results provide information on the reproductive state-dependent changes in the AVT system of female fishes, allowing important comparisons to the abundant literature on the role of AVT in male fishes. They also highlight the importance of detailed methods, adequate controls, and consideration of methodology (limitations, restrictions, advantages, etc.) when studying AVT or any neuropeptide/neurohormone system in nonmammalian organisms.

2 | MATERIALS AND METHODS

2.1 | Experimental animals

Laboratory-bred *A. burtoni* originated from a wild-caught stock from Lake Tanganyika, Africa in the 1970s and were maintained in an environment mimicking natural conditions (pH = 7.6–8.0; 28–30°C; 12L:12D diurnal cycle). Fish were fed cichlid flakes (AquaDine, Healdsburg, CA) daily and supplemented with brine shrimp twice weekly. Fish were housed in community aquaria (114 L) with gravel substrate and at least two to three terra cotta pots to serve as spawning territories for males. All experiments were performed in accordance with the recommendations and guidelines stated in the National Institutes of Health Guide for the Care and Use of Laboratory Animals, 2011. All animal care and collection were approved by the Institutional Animal Care and Use Committee at Louisiana State University, Baton Rouge, LA.

To examine differences in AVT expression across reproductive states, we collected gravid, mouthbrooding, and recovering females. Gravid females were selected based on the presence of a distended

abdomen, slightly distended jaw, and presence of actively courting males. Upon dissection, they were confirmed to have high levels of reproductive investment (i.e., gonadosomatic index, GSI, >7.0), and their ovulation status was recorded. Mouthbrooding females were collected 10–14 days after the onset of brooding, such that their brood were fully developed and females are more likely to exhibit aggressive behaviors (Field & Maruska, 2017). For comparison with late-stage brooding females, an additional group of mid-brooding females was collected 6–8 days after the onset of brooding. Recovering females were neither brooding nor gravid with GSI values ranging from 2.0 to 5.0, representing mid-cycle or ~2 weeks after brooding. Males were collected from community tanks, and their reproductive state was determined based on coloration, behaviors, and GSI (dominant >0.70; subordinate <0.50). A total of 30 fish were collected for staining purposes and 45 fish for qPCR analysis.

2.2 | Tissue collection and preparation

Animals were quickly netted from community aquaria, measured for standard length (SL; 40.483 ± 6.294 mm; mean ± *SD*) and body mass (BM; 1.754 ± 0.758 g), and sacrificed via rapid cervical transection. For staining, brains were exposed via craniotomy, fixed in 4% paraformaldehyde (PFA) in 1x phosphate buffered saline (1x PBS) overnight, rinsed twice in 1x PBS for ~24 hr each, and cryoprotected in 30% sucrose prepared in 1x PBS for >24 hr but no longer than 1 week. Brains were removed from the head between the two 1x PBS washes. Immediately prior to sectioning, cryoprotected brains were mounted in Optimal Cutting Temperature (OCT; Tissue-Tek, Torrance, CA) media and sectioned at 20 μm on a cryostat (Thermo Scientific HM525 NX). Of the 30 brains, 5 were sectioned in the sagittal plane but all others were coronal cross sections. Sections were collected onto alternate sets of superfrost plus microslides (VWR, Chicago, IL), dried flat at room temperature (RT) for 48 hr, and stored at −80°C in RNase-free conditions until further processing.

2.3 | Preparation of DIG-labeled riboprobes and ISH

To localize *avt* to specific regions of the brain, we used chromogenic ISH with gene-specific digoxigenin (DIG)-labeled riboprobes for the *A. burtoni avt/neurophysin* complex. Primer sequences were identical to previous studies in *A. burtoni* (Greenwood et al., 2008) and riboprobes were generated using previously described methods (Butler & Maruska, 2016; Grone & Maruska, 2015). Briefly, probe templates were amplified from whole brain *A. burtoni*, and DIG-labeled nucleotides (DIG RNA-labeling mix, Roche, Nutley, NJ) were then incorporated into the purified PCR product. Probes were purified (GE Illustra Probe Quant G-50 microcolumns), diluted, and stored at −20°C until use. Sense control probes were generated by adding the T3 recognition sequence (AATTAACCCTCACTAAAGGG) to the sense primer and generated as described above for antisense probes. All

steps were verified on agarose gels to have a single amplification product of the correct size, and the purified PCR product was sequenced (Eurofins Genomics) to verify probe specificity.

ISH was done following previously published protocols (Butler & Maruska, 2016; Grone & Maruska, 2015). RT slides of cryosectioned brains were treated with 1x PBS (3 × 5 min), 4% PFA (20 min), 1x PBS (2 × 5 min), proteinase K solution (10 min), 1x PBS, 4% PFA (15 min), 1x PBS (2 × 5 min), milliQ water (3 min), 0.1 M triethanolamine-HCl pH = 8.0 with acetic anhydride (10 min), and 1x PBS (5 min). Slides were then incubated for 3 hr in prehybridization buffer at 60°C before probe solution (probe diluted in hybridization buffer) was applied to slides, covered by hybrislips (Life Technologies), and incubated overnight at 60°C for ~18 hr. Following DIG probe incubation, slides were washed at 60–65°C in prewarmed 2x saline-sodium-citrate (SSC):50% formamide (2 × 30 min), 1:1 mixture of 2x SSC: maleate buffer (MABT; 2 × 15 min) and MABT (2 × 10 min). Slides were then washed at RT with MABT (2 × 10 min) and nonspecific binding was blocked with MABT containing 2% BSA for 3 hr. Following blocking, slides were incubated with anti-DIG antibody (Roche; 1:5,000 dilution; RRID: AB_514497) in blocking solution at 4°C overnight, flat, in a humidified chamber. Following incubation, slides were rinsed in MABT (3 × 30 min) at RT, washed in alkaline phosphatase buffer (2 × 5 min), and developed in NBT/BCIP (Roche) solution at 37°C for 1 hr. After development, slides were washed in 1x PBS (3 × 5 min), fixed in 4% PFA for 10 min, washed in PBS (3 × 5 min), coverslipped with aqueous mounting media (Aquamount, Lerner Laboratories), and allowed to dry on a flat surface overnight. A one-hr development time was used for all animals designated for cell counts and size. This time frame ensured that all cells stained, but that cell borders were more discernable from each other. Several animals were left to develop for ~24 hr to ensure that no additional staining (positive or background) would occur from prolonged development. To verify staining specificity, alternate sets of cryosectioned brains were stained simultaneously with the sense and antisense probes. Sense controls did not produce any labeling in the brain (Figure 1).

2.4 | Immunohistochemistry

To localize AVT cells and fibers, brains were stained with a primary antibody for AVT that was gifted from the Matthew Grober Lab (Georgia State University), was produced using an AVT Synpep coupled to keyhole limpet hemocyanin, and used in other fish studies (RRID:AB_2847958) (Dewan et al., 2008; Dewan et al., 2011; Loveland & Fernald, 2017; Maruska, 2009; Maruska et al., 2007). Slides of cryosectioned brains were brought to RT, outlined with a hydrophobic barrier, and rinsed in 1x PBS (3 × 10 min). After blocking nonspecific staining for 1 hr with 1x PBS containing 0.2% BSA, 5% normal goat serum, and 0.2% triton-x, slides were incubated in primary AVT antibody (1:2,000 prepared in blocking solution) overnight at 4°C, flat, in a humidified chamber. Slides were then washed in 1x PBS (3 × 10 min) and incubated in goat anti-rabbit IGg secondary antibody (1:267, dilution prepared in 1x PBS with 10% NGS; RRID: AB_2313606) for 1 hr. After sequential washes of 1x PBS
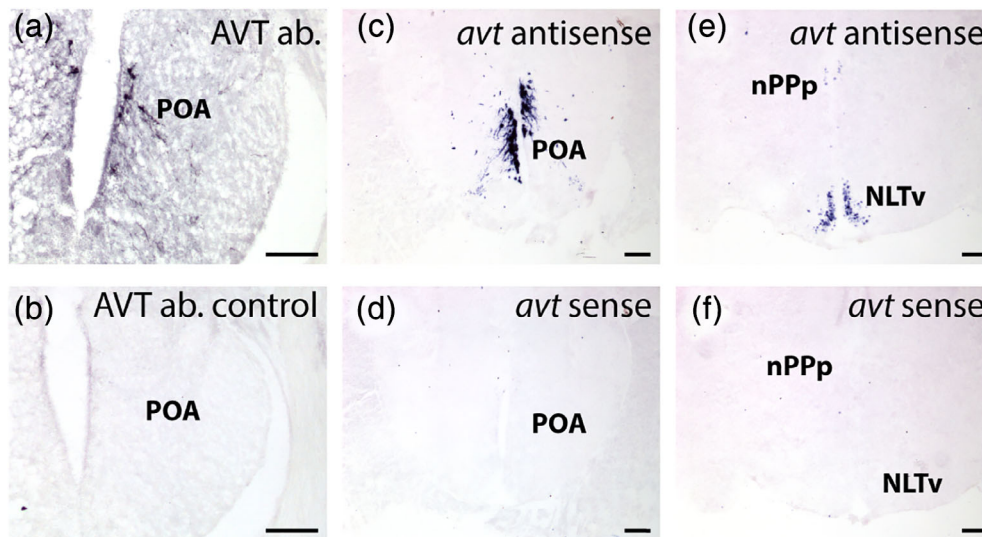
FIGURE 1 Representative photomicrographs of arginine vasotocin (AVT) antibody and in situ hybridization staining and controls. Antibody staining for AVT stains cell bodies in the preoptic area (POA) (a), but preabsorbing the antibody with AVT peptide eliminates staining (b). Riboprobe generated for *avt* mRNA results in stained cell bodies in several non-POA diencephalic regions (e). Hybridization with a sense control probe (T3 initiation sequence on forward primer instead of reverse) does not produce any staining (d,f). Scale bars = 100 μm. See list for abbreviations [Color figure can be viewed at wileyonlinelibrary.com]

(3 × 10 min), 1.5% hydrogen peroxide (10 min), and 1x PBS (3 × 10 min), slides were incubated in avidin–biotin-complex (ABC) solution (Vector labs; RRID:AB_2336827) for 2 hr at RT. Slides were then rinsed in 1x PBS (3 × 10 min) and reacted with DAB (RRID: AB_2336382) for ~5 min. After rinsing with DI water for 10 min, slides were dehydrated in an ethanol series and cleared in xylene before being coverslipped with cytoseal-60.

Preliminary studies were used to optimize primary and secondary antibody concentrations, as well as timeframe of secondary antibody and ABC reaction time. In addition, several brains were reacted for 30 min with DAB to ensure all cells and fibers were visible. Longer DAB reaction times had no impact on cell number or fiber density, and only increased intensity of the staining and darkened the background.

2.5 | Double fluorescent ISH–IHC

Several sets of slides were sequentially stained for both *avt*/AVT mRNA and peptide to better compare staining methods and expression of mRNA and protein in relation to each other. Double fluorescent ISH–IHC was performed according to previously published protocols (Butler & Maruska, 2019). Specifically, slides were first stained for *avt* mRNA using the chromogenic ISH protocol described above. On the final day of the ISH, slides were rinsed in MABT (3 × 20 min) and developed using SigmaFast Red instead of NBT/BCIP solution. All subsequent steps occurred in a dark, humidified sealed chamber. The reaction was stopped with 1x PBS washes (4 × 10 min) at RT, non-specific binding was blocked by incubating slides in 1x PBS containing 10% normal goat serum, 0.2% BSA, and 0.3% triton-X for 2 hr. After blocking, slides were incubated with AVT antibody (1:2,000) at 4°C for

12 hr. Slides were then washed in 1x PBS (3 × 10 min), incubated in Alexa Fluor 488 goat anti-rabbit antibody (1:500; RRID: AB 143165) for 2 hr in 1x PBS and 10% NGS, and washed in 1x PBS (3 × 10 min). Slides were coverslipped and cell nuclei counterstained with DAPI Fluorogel II (Electron Microscopy Services).

2.6 | Antibody characterization and controls

The following controls were performed to verify antibody staining specificity: (a) antibody was preabsorbed with twice the concentration of AVT peptide, (b) primary antibody was omitted, and (c) secondary antibody was omitted. Controls were run simultaneously on alternate sets of sectioned brain slides and showed no reaction product. We also preabsorbed the AVT antibody with twice the concentration of isotocin peptide, and staining was not qualitatively different from AVT antibody staining, indicating no cross-reaction with isotocin. In addition, double labeling for AVT peptide and *avt*-mRNA does not result in any AVT-peptide stained cells not co-labeled with *avt* mRNA. Western blots for AVT are technically challenging due to the small size (<2 kDa) of the peptide, and are not typically used to verify antibody specificity. This AVT antibody was also used in other teleost fishes, revealing similar staining patterns in the POA and hypothalamus (Dewan et al., 2008; Dewan et al., 2011; Maruska, 2009; Maruska et al., 2007; Ramallo et al., 2012).

2.7 | Imaging and analysis

Distribution of *avt*/AVT cells is based on consensus from brains in all animals. Because of apparent differences in mRNA and peptide

staining, results are presented separately. Stained slides were visualized on a Nikon Eclipse Ni microscope with color and monochrome digital cameras controlled by Nikon Elements software (RRID: SCR_014329). Chromogenic-reacted sections were viewed with a Nikon DS-Fi1 color digital camera in both brightfield and phase contrast for identification of neuroanatomical markers and visualization of cytoarchitecture. Nuclei identification is based on an *A. burtoni* brain atlas and relevant papers (Fernald & Shelton, 1985; Maruska, Butler, Field, & Porter, 2017), and a current consensus of nomenclature. However, some uncertainty remains regarding terminology and homologies of hypothalamic nuclei. Fluorescent slides were viewed and photographed with a Nikon DS QiMc monochrome digital camera. For each image, contrast, brightness, and levels were adjusted as needed, pseudocolored, and merged in ImageJ (imagej.nih.gov/ij/; RRID:SCR_003070). Autofluorescence and endothelial cell fluorescence were removed using the clone tool in photoshop (Adobe Systems, San Jose, CA; RRID:SCR_014199) for visualization purposes.

Cells containing either *avt* mRNA or AVT protein were quantified for cell size and number in gravid and brooding females. Only subsets of animals (between 35 and 45 mm SL) were quantified for cell count and cell number analysis. For IHC data, eight ovulated females, three mid-brood females, and six late-brood females were analyzed. For ISH data, four ovulated and four late-brood females were analyzed. In AVT IHC stained brains, the total number of parvocellular, magnocellular, and gigantocellular cells were quantified in all regions of the POA. We classified cells within each population by size (i.e., parvocellular = ~5 μm diameter, magnocellular = ~10 μm diameter, gigantocellular >10 μm diameter), and not location (i.e., nMMp, nPMp, etc.). The number of stained cells was counted throughout the rostrocaudal extent of the POA in each animal from 20 μm alternate sections collected on a single slideset. Cell size was quantified in a subset of parvocellular, magnocellular, and gigantocellular cells by randomly selecting up to 10 cells of each group per animal. Extended depth of field images were taken at ×40 of all animals using the same brightness and contrast settings. Images were then loaded into ImageJ, converted to gray scale, and a threshold was used to isolate cells. Cell area (in μm^2) was then calculated using ImageJ's measuring tools. Neurons were only selected if their borders were completely discernable (i.e., no overlap with neighboring stained cells). An average parvocellular, magnocellular, and gigantocellular cell size was calculated for each animal. Similar methods were used for analyzing cell number and size in *avt* ISH stained brains. In addition to the POA, cell size and number were also collected for other diencephalic cell groups (i.e., NLTv/ventral tuberal nucleus [VTn] area; PGa area).

Because of differences in cell size between reproductive states, we applied the Abercrombie correction to cell count data (Abercrombie, 1946). Average cell diameters were calculated for each animal group, cell type, and staining method. Corrected cell counts were calculated $(T/(T + CD)) \times CN$, where T is section thickness (20 μm), CD is cell diameter, and CN is cell number. Corrected and uncorrected cell counts yield the same results, and only corrected cell counts are presented in the results section and figures.

2.8 | mRNA expression via quantitative RT-PCR

A separate set of animals was used to examine *avt* mRNA levels via quantitative PCR. Gravid, brooding, and recovering females were identified from community tanks as described above in Section 2.1 and as part of another study (Maruska, Butler, Anselmo, & Tandukar, 2020). Immediately after sacrifice, the brains were quickly dissected from the head, embedded in OCT media, frozen on dry ice, and stored at −80°C until processing. Brains were sectioned in the transverse plane at 300 μm on a cryostat and collected onto charged slides, which were stored at −80°C until microdissection. Microdissections were done as described in (Maruska et al., 2020). Briefly, slides were placed on a frozen stage (BFS-30MP, Physiotemp Instruments) and viewed through a dissection microscope. Samples were collected into lysis buffer with a modified 23G needle (inner diameter = 360 μm) attached to a syringe. Samples were collected onto dry ice and stored at −80°C until RNA isolation (Qiagen, RNeasy Micro Plus). Microdissections were taken from the medial part of the dorsal telencephalon (Dm; pallial amygdala homolog, in part), supracommissural part of the ventral telencephalon (Vs, basal/extended amygdala homolog, in part), and POA. To minimize variation in sampling, all 36 individuals were sampled by the same individual experimenter. The same amount of tissue was collected from each animal in each region (i.e., both right and left hemispheres, same number of sections).

RNA was isolated according to manufacturer's protocol, reverse transcribed into cDNA (QuantBio qScript cDNA supermix), and diluted in RNase-free water. Quantitative RT-PCR was then used to measure mRNA levels of *avt* and two reference genes (*gapdh* and *eef1a*). qRT-PCR was done as previously described (Butler et al., 2019; Maruska et al., 2020) with samples run in 20 μl duplicates on a CFX Connect System (BioRad). The same primer sets were used for qRT-PCR and ISH probe generation, just without the T3 initiation sequence. Reaction parameters were 95°C for 30s, 45 cycles of 95°C for 1 s and 60°C for 15 s, followed by a melt curve analysis. Cycle threshold and reaction efficiencies were calculated in PCR miner (Zhao & Fernald, 2005). Data were normalized to the geometric mean of the reference genes, and relative expression was calculated as: relative target gene mRNA levels = $[1/(1 + E_{target})\wedge CT_{target}]/[1/(1 + E_{geomean})\wedge CT_{geomean}] \times 100$, where E is the reaction efficiency and CT is the average cycle threshold of the duplicate wells. Reference gene expression did not differ among the groups (tested via analysis of variance [ANOVA]), all primers had a single melt peak, and sequencing was used to verify amplification of only *avt* transcripts.

2.9 | Statistical analysis

All statistics were performed in SigmaPlot 12.3 (RRID:SCR_003210). Data were first checked for normality, equal variance, and outliers. If normality or equal variance was not met, transformations were used (i.e., log, natural log, or square root). Outliers were removed as appropriate. To compare cell number and size in the POA, we used a two-way repeated measure ANOVA with cell type (parvocellular,

magnocellular, and gigantocellular) as a repeated measure and reproductive state (gravid or brooding) as a fixed factor. We also used student's *t* tests to compare gravid and brooding groups within each cell type to further examine if cell number and size varied with reproductive state independent of other cell types. For other diencephalic cells, we used student's *t* tests to compare gravid and brooding females. To compare cell number and size differences between the two methodologies, a two-way repeated measure ANOVA was used with method (ISH or IHC) and reproductive state as the two factors. A repeated measures test was used since IHC and ISH stains were performed on alternate slide sets of the same brains. We ran all statistics on body-size corrected and uncorrected data. Correcting for body size (using SL, BM, or both) had no impact on statistical significance, so only statistics on uncorrected data are presented. All data are presented as mean ± *SD* and Tukey's box plots are used for data representation. The box extends to the furthest data points within the 25th and 75th percentiles. Whiskers extend to the furthest data points within ×1.5 the interquartile range, and outliers (beyond ×1.5 the interquartile range) are designated by open circles and are not reflective of statistical outliers. Data mean is represented by a filled circle and data median by a solid line.

3 | RESULTS

Throughout the text, standard gene notations are used. When discussing mRNA staining detected via ISH, *avt* is used. In contrast, AVT-ir is used for peptide staining via IHC. When speaking generally about the system, we use AVT. Brains from gravid, brooding, and recovering females, and subordinate and dominant males were used for a comprehensive localization description. In some instances, cells were qualitatively different between males and females, and are described below as appropriate.

3.1 | Distribution of *avt*-expressing cells

All animals had *avt*-expressing cells in all subdivisions of the POA (Figure 2). Abundant parvocellular cells are observed in the nPPa and

FIGURE 2 Representative photomicrographs of *avt*-expressing cells in the *A. burtoni* brain. *avt*-Expressing cells bodies are found throughout all subdivisions of the preoptic area in parvocellular (a–c), magnocellular (d,e), and gigantocellular cells (f). No *avt*-stained cells are present anywhere in the telencephalon (b). *avt*-Expressing cells are also found along the third ventricle in the ventral subdivision of lateral tuberal nucleus (NLTv) (g,h,j,l) and in the area of the preglomerular complex (g,h). Cresyl violet images (a,d,e) correspond to the approximate locations of the images in each row and shown in (i). Images are of cross sections (b–h) and sagittal (j–l) sections. Scale bars = 250 μm (a c,h); 100 μm (b,e,g,d inset). See list for abbreviations [Color figure can be viewed at wileyonlinelibrary.com]
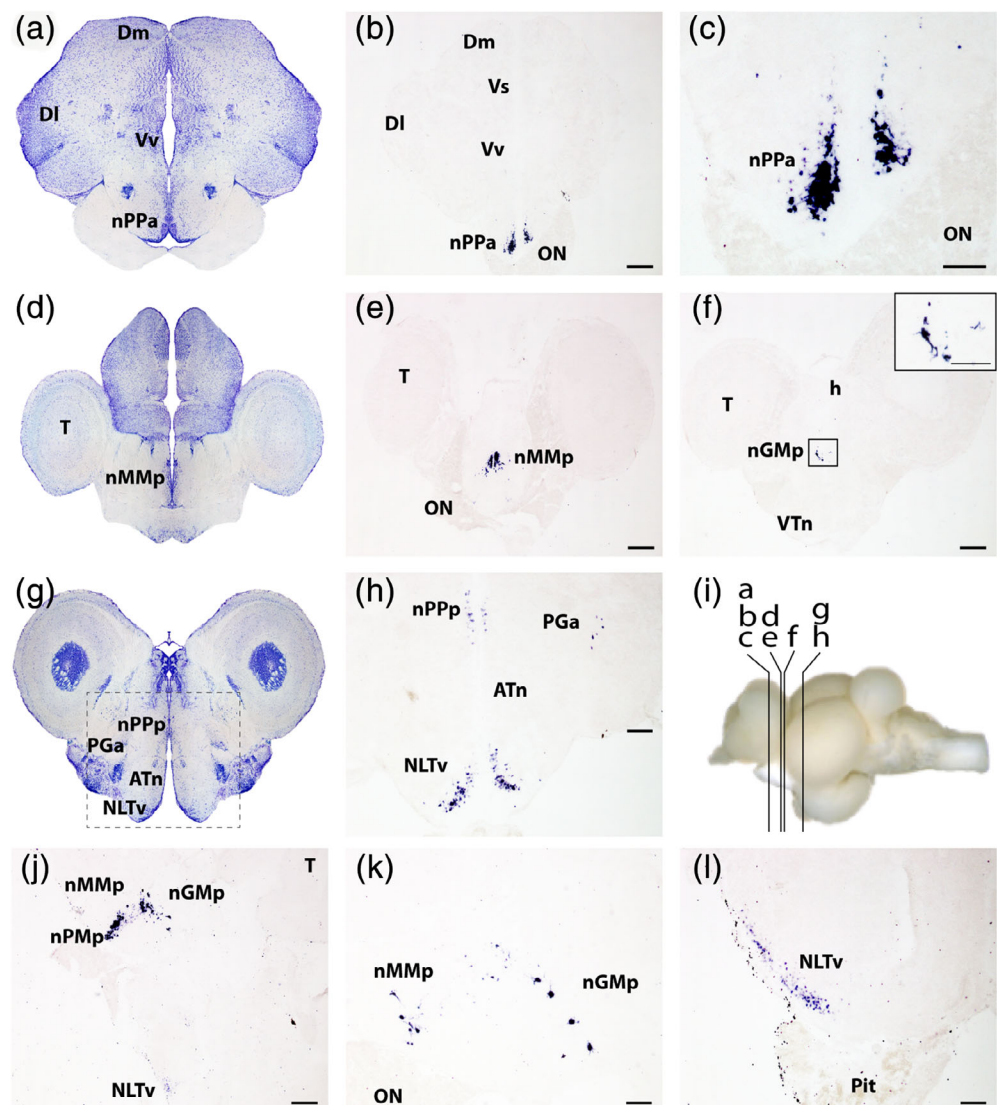
nPPp subdivisions and scattered throughout the nMMp and nPMp subdivisions (Figure 2a-c). Magnocellular *avt*-stained cells populate the nMMp, nPMp, and nGMp divisions (Figure 2d,e). Gigantocellular cells expressing *avt* are only found sparsely throughout the nGMp subdivision (Figure 2g). Based on sagittal staining, cells appear rostrally in the nPPa subdivision and arc dorsally and caudally (Figure 2j,k). Parvocellular cells do not appear to have any stained processes revealed by *avt* ISH, but magnocellular cells typically have one to two stained process and gigantocellular cells often have numerous stained processes. As such, mRNA-containing axon varicosities are found occasionally within the POA, particularly in the fiber bundle known to project to the pituitary.

Avt-expressing cells also lie along the ventral midline of the hypothalamus in the area of the lateral tuberal nucleus (NLT) and VTn (Figure 2h,j,l). Hypothalamic cells appear similar in size to parvocellular preoptic cells, are more lightly stained than POA cells, and do not show any stained processes with ISH. These cells appear more caudal than where the VTn was previously described in *A. burtoni* (Munchrath & Hofmann, 2010; O'Connell, Fontenot, & Hofmann, 2011). The cells lie on the medioventral edge, which is typically indicative of the ventral NLT subdivision (NLTv) rather than VTn (Porter, Roberts, & Maruska, 2017). No stained cells are seen in the anterior tuberal nucleus (ATn). In close proximity to the ATn, *avt*-expressing cells lie along the midline in the nPPp. The hypothalamic cells are abundant in all females. While all males possessed *avt*-expressing cells in this region, qualitative comparisons showed they had fewer than females.

In addition, a separate group of *avt*-stained cells are observed in a lateral portion of the diencephalon. In both sagittal and cross-sectioned brains, these cells appear near or within the preglomerular complex, potentially in the anterior portion, PGa (Figure 2h). Staining in this region is present in all females, but is only observed in 50% of dominant males and no subordinate males. These cells appear similar in size to parvocellular preoptic cells and do not have any obvious stained processes.

No other *avt* cellular staining is visible in any part of the brain, even in slides left to develop for 24 hr as opposed to the normal 1 hr. No *avt*-stained fibers are visible outside of those immediately adjacent to darkly stained POA cells. The telencephalon is completely devoid of any *avt* mRNA staining.

3.2 | Distribution of AVT-ir cells and fibers

All animals have AVT-ir cell bodies in all subdivisions of the POA revealed by immunohistochemical staining for protein (Figure 3). AVT-ir revealed unipolar parvocellular cells are in the nPPa, nPPp, nMMp, and nPMp subdivisions (Figure 3a,b). Magnocellular cells lie more along the midline in the nPMp, nMMp, and nGMp subdivisions with many appearing as bipolar (Figure 3c,d). Multipolar gigantocellular cells are located throughout the nGMp subdivision (Figure 3e,f). Darkly-stained fibers are often seen extending from AVT-ir POA cells. No other AVT-ir cells are observed in any part of the brain. Despite increased antibody concentrations and reaction times, no additional staining was observed even in areas where *avt* mRNA is present such as the NLT and PGa.

AVT-ir fibers and varicosities are located throughout the brain. No fibers are seen in the olfactory bulbs, and little to no fibers are observed in dorsal telencephalic nuclei (e.g., Dm, Dc, Dl), with the exception of some scattered fibers in dorsal Dd. In contrast, AVT-ir fibers lie throughout ventral telencephalic nuclei including Vv (Figure 3h), Vl, Vc, Vd, and Vs. A varicosity-dense fiber tract (preoptico-hypophyseal tract) extends from the POA and runs along the ventral border of the hypothalamus to the pituitary (Figure 3g). The pituitary was also dense with AVT-ir fibers. Fibers are found lateral to the periventricular nucleus of the posterior tuberculum and in central and dorsal thalamic nuclei (CP, DP), habenula, nucleus of the lateral recess, and NLT (Figure 3i). In the midbrain, fibers are scattered in the torus semicircularis where they are more abundant in caudal sections (Figure 3j). Fibers also lie in the tegmentum and are abundant along the midline in the regions medial to Gn and dorsal to PGc. Few AVT-ir fibers were seen in the tectum. In the rhombencephalon, the most obvious fibers were present along the ventral hindbrain beneath the medial longitudinal fasciculus (mlf) and around the reticular formation nuclei, and these fibers extended into the spinal cord. A distinct AVT-ir fiber tract was also seen projecting through the midbrain to the medulla in a lateral rostrocaudal position just above the tectobulbar tract (Figure 3k). This fiber tract then projected dorsally near the lateral lemniscus and into the regions of the caudal torus semicircularis, paratoral tegmental nucleus, and medial part of the perilemniscular nucleus. AVT-ir fibers also lie in the region of the descending tract of the trigeminal nerve (Vde) and secondary gustatory tract (sgt) throughout their rostrocaudal lengths. No fibers were seen in the cerebellum.

3.3 | Cell number does not vary with female reproductive state

We quantified each cell type (parvo-, magno-, and gigantocellular) independently and regardless of POA subdivision location, instead focusing on cell type. Cell types were identified based on morphology (i.e., size and projections) and location. Overall, parvocellular cells are most abundant and gigantocellular cells are least abundant. However, there is no significant effect of reproductive state on the number of AVT-ir or *avt*-containing cells in the POA (Figure 4a,b; AVT-ir: reproductive state: $F_{1,50} = 0.343$; $p = .576$; cell type: $F_{2,50} = 123.575$; $p < .001$; state × type: $F_{2,50} = 0.012$; $p = .988$; *avt*: reproductive state: $F_{1,23} = 0.149$; $p = .724$; cell type: $F_{2,23} = 184.398$; $p < .001$; state × type: $F_{2,23} = 1.050$; $p = .406$). The total number of AVT-ir and *avt*-mRNA containing cells in the POA is not different between the reproductive states ($p > .05$ for both). Similarly, ovulated and brooding females have similar numbers of *avt*-expressing cells in the NLTv area ($p = .214$; Figure 6a) and diencephalic region near the PGa ($p = .616$).

3.4 | Cell size varies with female reproductive state

For both AVT-ir and *avt*-mRNA containing cells, cell size was significantly different across each cell type with parvocellular cells being the
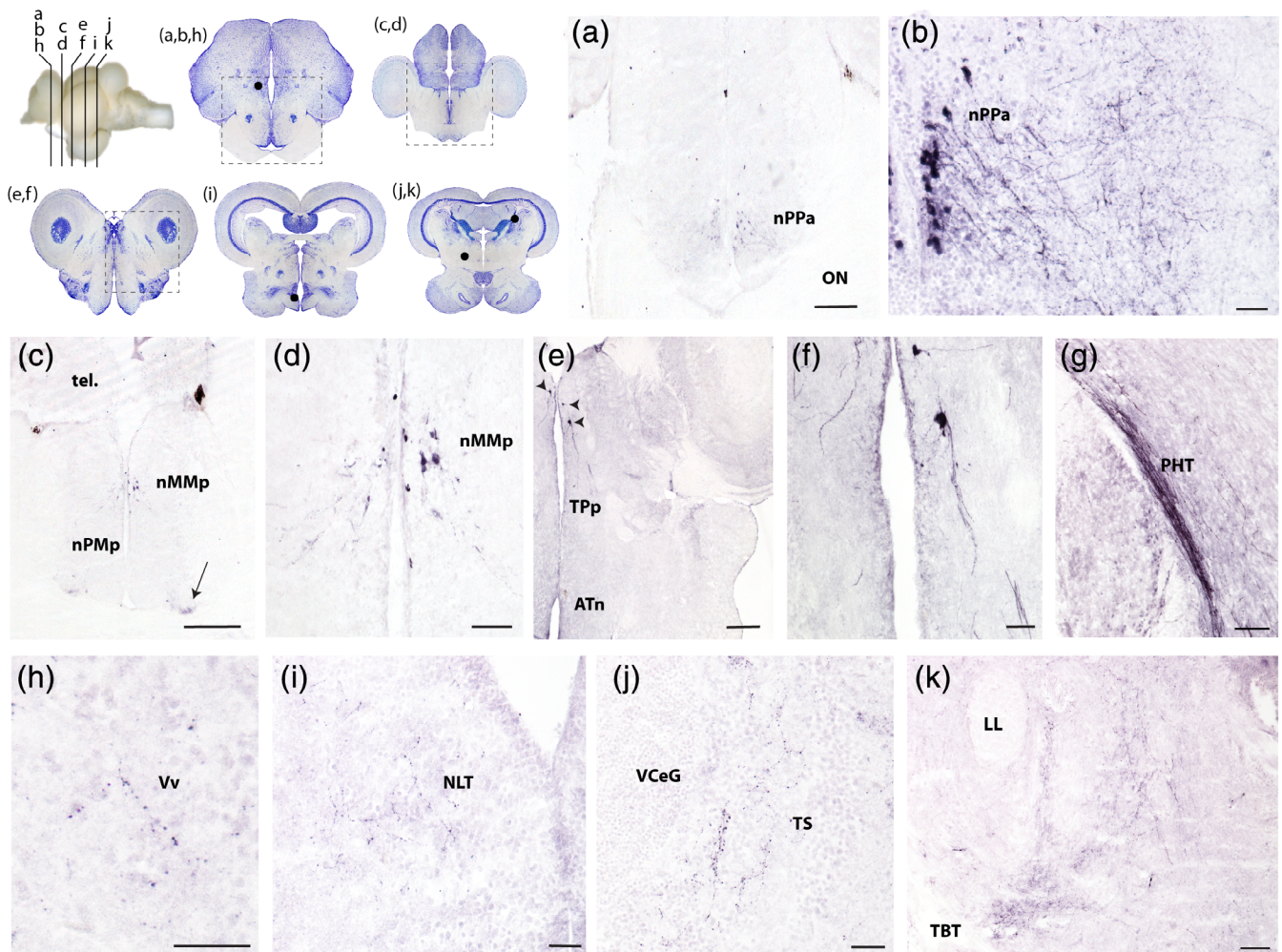
FIGURE 3 Photomicrographs of arginine vasotocin (AVT)-immunoreactive staining in the preoptic area (POA). AVT-stained cells are located throughout the entire POA. Parvocellular cells contain single projections, often extending laterally or ventrally to create a tract toward the pituitary (a,b). Magnocellular (c,d) and gigantocellular (e,f) stained cells often have several processes extending away from the cell body. Arrow in (c) indicates fiber tract. Arrow heads in (e) denote AVT-ir cells magnified in (f). A fiber tract extends from the POA to the pituitary (g). AVT-ir fibers are found in the ventral telencephalon (h), lateral tuberal nucleus (i), caudal torus semicircularis (j) and hindbrain (k), among other regions. The approximate locations of images are shown in the first panel with corresponding images of cresyl violet staining. Dashed boxes on cresyl violet images represent the approximate location of each image showing AVT-ir labeled somata while the black dots represent approximate locations of each image showing AVT-ir varicosities. Scale bars = 250 μm (a,c,e); 50 μm (d,f,k), 25 μm (b,g–j). See list for abbreviations [Color figure can be viewed at wileyonlinelibrary.com]

smallest and gigantocellular cells being the largest (Figure 4c,d). While no differences were observed in *avt*-expressing cell sizes in the POA, there were reproductive state differences in AVT-ir peptide containing cell body sizes in the POA (reproductive state: $F_{1,23} = 0.163$; $p = .714$; cell type: $F_{2,23} = 164.500$; $p < .001$; state × type: $F_{2,23} = 0.602$; $p = .578$). However, ovulated females have significantly larger POA AVT-ir cells than brooding females, independent of cell type. Using student's t tests to compare ovulated and brooding cell sizes within each type independent of each other, we found that ovulated females have larger magnocellular ($p < .001$) and gigantocellular ($p = .011$) cells than brooding females.

Within gigantocellular AVT cells, late-stage brooding females have larger cells than mid-stage brooding females ($p = .002$; Figure 5a), and soma size positively correlates with the number of days brooding ($R = .881$, $p = .003$; Figure 5b). There are no reproductive state differences in parvocellular AVT-ir soma size ($p = .195$), and brooding state (middle vs. late), did not influence magnocellular ($p = .631$) or parvocellular ($p = .098$) AVT-ir soma size.

In the NLTv, brooding females have larger *avt*-containing cells compared to ovulated females ($p = .006$; only late-stage brooding females were used for this analysis; Figure 6b). There are no reproductive state differences in the *avt*-containing cell sizes of the diencephalic cell group ($p = .634$).

3.5 | Comparison of mRNA and peptide staining for AVT/*avt*

Using brains double-labeled with ISH–IHC and brains with alternate slides stained with AVT and *avt*, comparisons between ISH and IHC
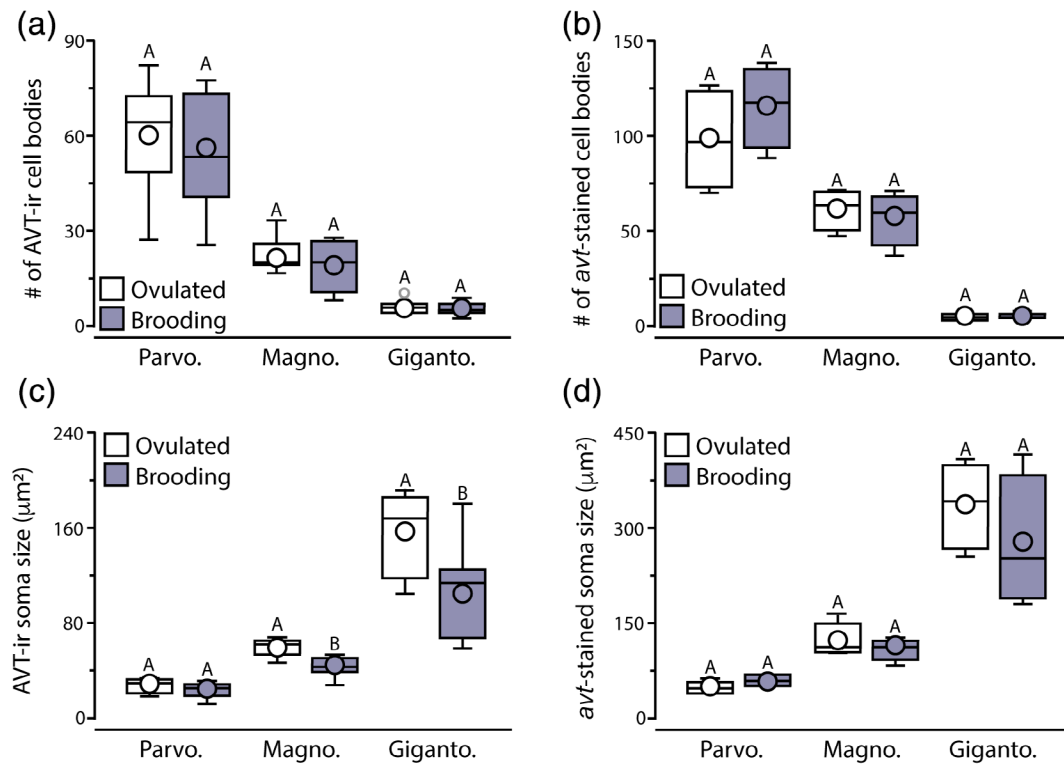
FIGURE 4 Arginine vasotocin (AVT)-ir cell size but not number varies with female reproductive state. Ovulated and brooding female brains have similar numbers of AVT-ir (a) and *avt*-expressing (b) cells. Cell type was classified based on morphology and location, with the Abercrombie correction applied to cell counts. Ovulated females have larger AVT-ir magnocellular and gigantocellular cells (c), but soma size of *avt* stained cells does not vary with reproductive state (d). Note the difference in y-axes between (a) and (b) and between (c) and (d), showing differences between immunohistochemistry (IHC) and in situ hybridization (ISH) staining. Parvo, parvocellular cells; Magno, magnocellular cells; Giganto, gigantocellular cells. Different letters indicate $p < .05$. $N = 9$ per group (a,c); 4 per group (b,d). Middle and late brooding females are combined for (a,c), but only late-stage brooding females are included in (b,d). See Section 2 for boxplot descriptions [Color figure can be viewed at wileyonlinelibrary.com]
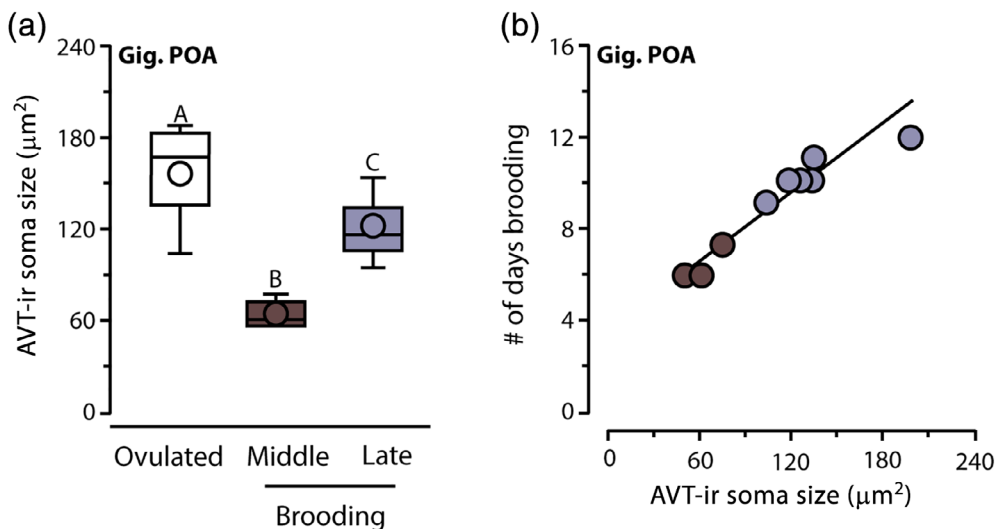

FIGURE 5 Gigantocellular arginine vasotocin (AVT)-ir soma size varies with length of time brooding. Late brooding (10–12 days) females have larger AVT-ir gigantocellular cells than mid-brood (6–8 days) females, but both are smaller than ovulated females. AVT-ir gigantocellular cell size positively correlates ($R = .881$, $p = .003$) with number of days brooding. Different letters indicate $p < .05$. $N = 9$ gravid, 3 mid, 6 late brooding females. See Section 2 for box plot descriptions [Color figure can be viewed at wileyonlinelibrary.com]

methodologies can be more directly observed (Figure 7). The only fibers with *avt* staining were observed in the immediate vicinity of densely stained POA cells (Figure 7e). AVT-ir fibers were much more numerous and widely distributed than fibers with *avt* mRNA. No mRNA staining was observed in the telencephalon in the vicinity of the AVT-ir fibers. No AVT-ir cells were observed anywhere in the brain outside of the POA.

Overall, animals had more and larger *avt*-containing cells than AVT-ir cells (number: $F_{1,23} = 21.320$; $p < .001$; size: $F_{1,23} = 18.283$;
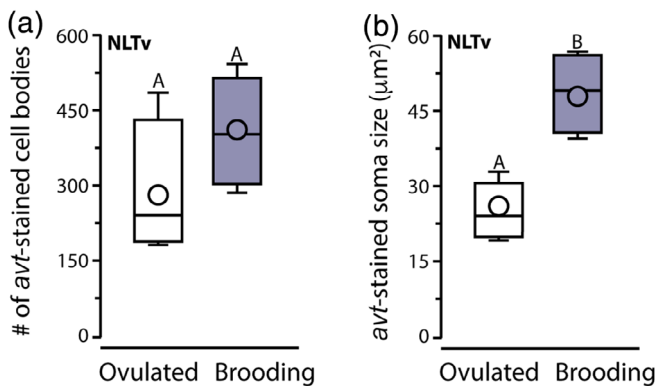
FIGURE 6 Size of *avt*-expressing cells in the ventral subdivision of lateral tuberal nucleus (NLTv) varies with female reproductive state. Ovulated and brooding (only late-stage brooding females included for in situ hybridization [ISH]) have a similar number of *avt*-mRNA stained cells (a), but *avt*-expressing cells in brooding females are larger than those in ovulated females (b). Different letters indicate $p < .05$. $N = 4$ per group. See Section 2 for box plot descriptions [Color figure can be viewed at wileyonlinelibrary.com]

$p = .003$). On average, females had approximately two-thirds fewer AVT-ir POA somata compared to *avt* somata. AVT-ir POA somata, on average, were also about half the size of *avt* stained cell bodies.

3.6 | mRNA levels measured via quantitative PCR did not differ across female reproductive states

To further analyze *avt* mRNA levels, we microdissected the medial part of the dorsal telencephalon (Dm), supracommissural nucleus of the ventral telencephalon (Vs), and the POA from gravid, brooding, and recovering females. Expression was dependent on brain region ($F_{2,107} = 20.026$; $p < .001$), but not reproductive state ($F_{2,107} = 1.444$; $p = .257$) and there was no interaction between region and state ($F_{4,107} = 1.519$; $p = .213$; Figure 8). Gravid, brooding, and recovering females had similar levels of *avt* mRNA in each region. However, POA *avt* expression was ×100 higher than that measured in the Dm and almost ×10,000 higher than expression in the Vs.

4 | DISCUSSION

The nonapeptide AVT is well studied for its role in mediating reproductive and aggressive behaviors in a variety of species, especially fishes. However, these studies are mostly limited to males or sex-changing fishes, with little attention to the AVT system of female fishes. Here, we described AVT expression in the brain of female *A. burtoni*, a model system where *avt* expression was previously described in males, but with differing results dependent on the study. Further, we used multiple techniques for identifying and quantifying AVT/*avt* expression, which produced different results. Despite a recent report (Rodriguez-Santiago et al., 2017), we found that *avt*-

mRNA expressing cells were restricted to the POA and ventral hypothalamus, which is consistent with studies in the overwhelming majority of other teleosts examined to date. In addition, we found that AVT-ir cell size in the POA varied with female reproductive state, but AVT-ir and *avt*-containing cell number, *avt* soma size, and mRNA levels measured via qPCR did not differ across female reproductive state. When combined with detailed work on the AVT system in male *A. burtoni*, these data provide one of the most comprehensive pictures of the AVT system in teleosts and offer relevant insights on the evolution of nonapeptide systems and their role in social behaviors.

4.1 | Distribution of avt/AVT-containing cells

As previously reported in *A. burtoni* and most teleosts examined to date, we found AVT cell expression throughout the POA and in the ventral hypothalamic regions. AVT was detected in parvocellular, magnocellular, and gigantocellular cells in the POA using both IHC and ISH. These POA *avt*-containing cells are ubiquitous across fishes, with all fishes thus far having AVT cells in the POA that project widely throughout the brain (Godwin & Thompson, 2012; Kagawa et al., 2016; Saito et al., 2004). In addition to the preoptico-hypothalamic AVT cells, we localized *avt*-containing cells to two regions of the diencephalon. A rather large cell group was found in the ventral hypothalamus, near the ventral subdivision of the NLTv. A previous study in *A. burtoni* also localized these to the NLT (Greenwood et al., 2008); however in other fishes, this cell group was described as part of the VTn, and in midshipman, *avt*-expressing cells were also found in the ATn (Goodson et al., 2003). Goodson et al. (2003) note that this ATn cell group was not present in all individuals, and were especially absent or hard to detect in reproductive animals from summer months. While we found cells in close proximity to the ATn, we believe these were part of the caudal extent of nPPp based on cytoarchitecture observed by cresyl violet staining. However, the cells we observed near the PGa could represent a similar population, and were similarly not equally expressed across all animals. Ventral diencephalic cells in *A. burtoni* were present more frequently in females than in males. Further research is needed to determine if these AVT cells located outside of the POA are universally expressed in teleosts, and if there are species, sex, and status-dependent expression patterns, which appears to be the case.

It was previously reported that *avt* preprohormone mRNA (simplified to *avt* in this study) is expressed ubiquitously throughout the telencephalon of *A. burtoni* ((Rodriguez-Santiago et al., 2017) but see (Loveland & Hu, 2018)). Using the same in situ probe sequence, we did not find any *avt* staining in the telencephalon (Table 1). Even when left to develop for over 10 times longer than normal, no staining was present in the telencephalon. The authors argue the reason no one else has observed this is due to "ascertainment bias" where past scientists did not examine the telencephalon for *avt*-mRNA expressing cells. Here, we do not discuss telencephalic *avt* cells because none were detected, which is likely also the case in past studies where AVT expression in the telencephalon was not discussed. There are several
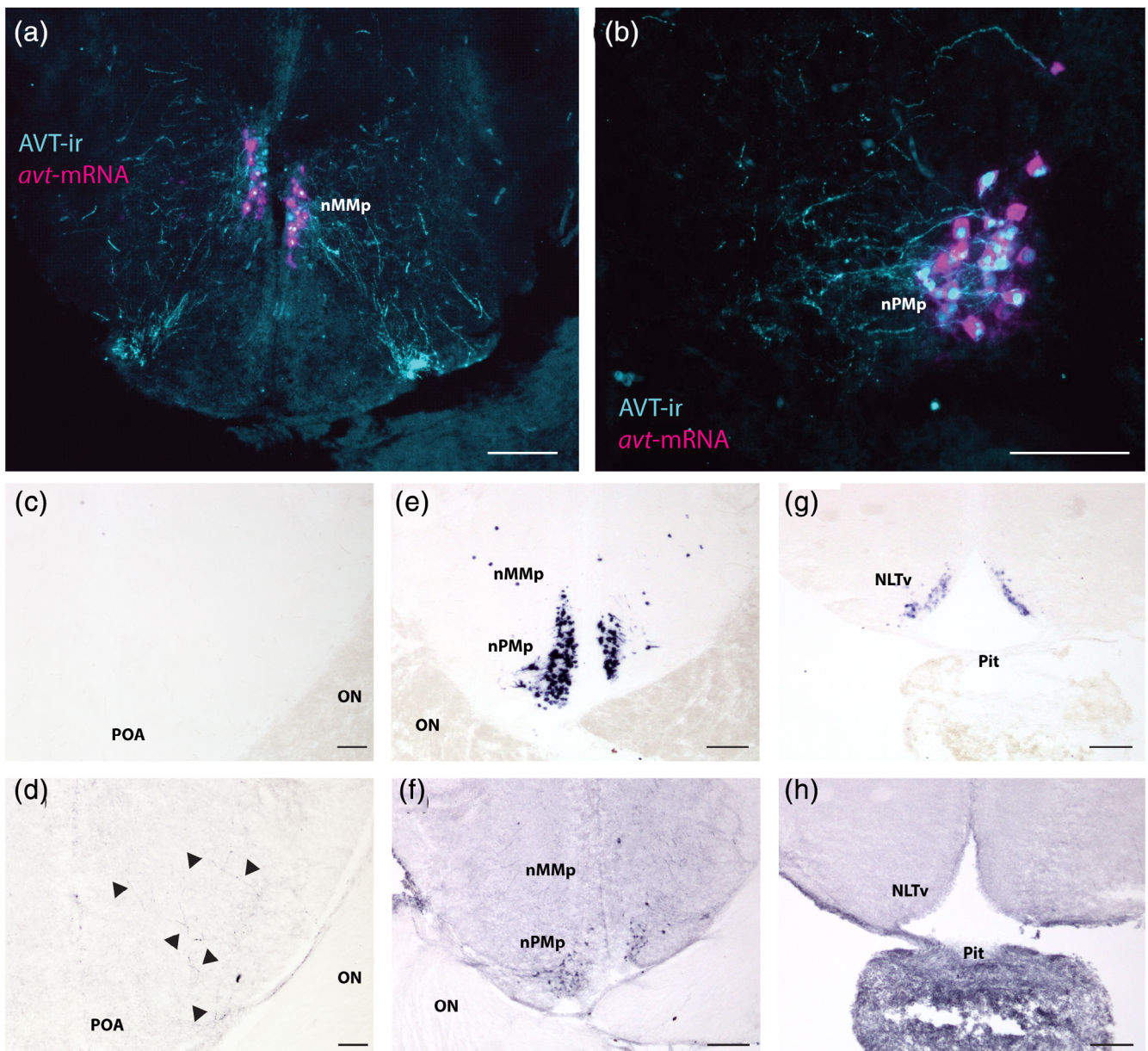
FIGURE 7 Comparisons of arginine vasotocin (AVT)-ir and *avt* staining using dual labeling and staining of alternate slide sets. In the preoptic area (POA), AVT-ir somata colocalize with *avt*-containing cells (a,b). Despite AVT-ir fibers in the POA (arrowheads in d), there is not *avt*-stained fibers (c). *avt*-containing cells are more abundant than AVT-ir cells throughout the POA (e,f). In the ventral hypothalamus, *avt*-containing cells line the ventricle (g), but no AVT-ir (h) cells are present. Scale bars = 100 μm (a,e,f,g,h); 50 μm (b,c,d) [Color figure can be viewed at wileyonlinelibrary.com]

possible explanations for the differences in staining results between these two studies, most stemming from differences in methodology. Many of the potentials pitfalls from the previous study have been outlined and discussed in a commentary by Loveland and Hu (2018), including insufficient ISH controls, insufficient qPCR controls such as positive and negative controls, and possible genomic DNA contamination. While we used the same primer sequences to generate probes for ISH, we used different hybridization conditions, stronger stringency washes, and developed with NBT/BCIP as opposed to BM purple, which can produce hazier staining. Poor hybridization conditions, combined with weaker stringency washes and the use of BM purple could result in nonspecific probe hybridization and diffuse, nonspecific

staining. As such, we argue that despite this recent report, *avt* expression is not present in the telencephalon of *A. burtoni*, but rather, predominately restricted to the POA and ventral hypothalamus in fishes, as previously documented in this species (Table 1) and the vast majority of AVT studies in teleosts.

4.2 | AVT expression varies with female reproductive state

Based on manipulation studies using either AVT injections or receptor antagonists, it is well accepted that AVT plays a role in motivation of
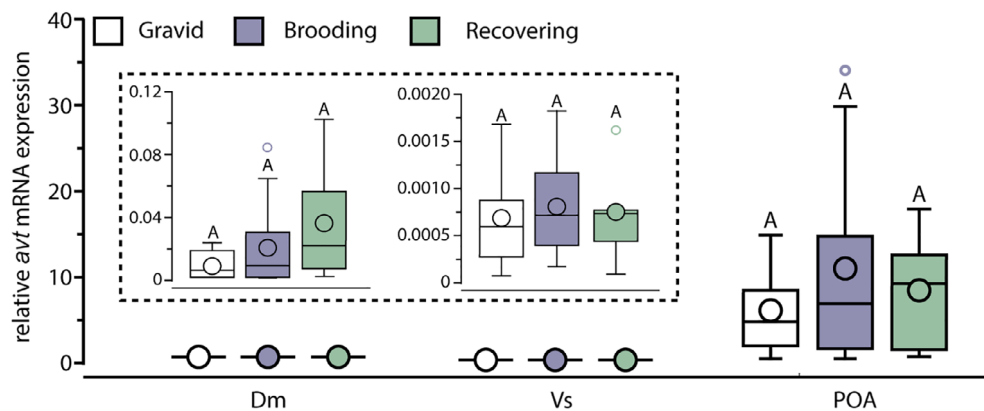
FIGURE 8 qRT-PCR analysis of *avt* mRNA in Dm, Vs, and POA. Relative expression of *avt* mRNA does not differ among gravid, brooding, and recovering females in the Dm, Vs, or POA. Expression of *avt* is ~×100 and ×10,000 lower in the Dm and Vs, respectively, when compared to POA expression. Inset of Dm and Vs is on a different scale for visualization purposes. Similar letters indicate $p > .05$. $N = 12$ per group. See Section 2 for boxplot descriptions. Dm, medial part of the dorsal telencephalon; POA, preoptic area; Vs, supracommissural nucleus of the ventral telencephalon [Color figure can be viewed at wileyonlinelibrary.com]

mating-related behaviors, including modulation of territorial behaviors, display of courtship behaviors, and social status (Godwin & Thompson, 2012; Semsar, Kandel, & Godwin, 2001). Historically, studies have largely focused on the role of nonapeptides in males, likely because of their overt and more easily quantified and documented social behaviors compared to females. However, results in males cannot and should not be extended to females, and more studies are needed to not only examine expression patterns of neuropeptides in females, but also functionally test them in females compared to males. When comparing male and female *A. burtoni*, there were no qualitative differences in POA AVT staining, but non-POA diencephalic cells were more abundant in females than in males. In midshipman fishes, females have a similar number of AVT-ir neurons to type I males (large nest-guarding, parental), and both type I males and females have more AVT-ir neurons than type II males (small sneaker), but this can be largely explained by the larger body size (Foran & Bass, 1998). Interestingly, in the blenniid fish *Salaria pavo*, females almost completely lacked AVT-ir parvocellular cells in the POA (Grober, George, Watkins, Carneiro, & Oliveira, 2002), which was attributed to the lack of female subordination behaviors by this species. However, we found robust parvocellular AVT expression in females, and this did not vary by female reproductive state. In gobies, AVT-ir varies with both sex and seasonality in a cell-type specific manner (Maruska et al., 2007). While very few differences in cell size and number were found in males across different seasons, both cell number and cell size varied in females such that females at peak-spawn and nonspawn times had more and larger cells that females at other time points. This suggests that in females, AVT production may be associated with physiological status and egg development, ovulation, and steroid hormone production. Further, in female round gobies, perfusion with 17β-estradiol over explanted brains increased AVT release, and acted through both genomic and nongenomic pathways (Kalamarz-Kubiak et al., 2017), and gonadal steroids, particularly estrogens, mediate AVT production and expression across taxa (Boyd, 1994; Miller et al., 1989; Sladek &

Somponpun, 2008). Gravid, ready-to-spawn *A. burtoni* females have higher circulating estradiol concentrations (Butler et al., 2019; Maruska et al., 2020; Maruska & Fernald, 2010) and higher expression of aromatase (Maruska et al., 2020), an estrogenic enzyme, compared to recovering and mouthbrooding females. This, combined with the expression of estrogen receptors in both the preoptic area and ventral hypothalamus (Munchrath & Hofmann, 2010), suggest that increased estrogen signaling in the brain could mediate increases in AVT observed here.

We did not find any reproductive-state differences in the number of AVT-ir or *avt* containing cells in the preoptic area or ventral hypothalamus. However, cell size varied with female reproductive state, suggesting that in at least *A. burtoni*, it is not how many AVT neurons are present but how much peptide those neurons are making and releasing that is important. In the preoptic area, we found that magnocellular cell size was larger in gravid compared to brooding females. Magnocellular AVT cells are proposed to be involved in neural circuitry mediating aggressive interactions (Larson, O'Malley, & Melloni Jr, 2006) and in male *A. burtoni*, magnocellular AVT cells are differentially activated during aggressive interactions compared to courtship and control conditions (Loveland & Fernald, 2017). In the laboratory setting, females can be aggressive, especially toward other females, with reproductive state being one of the main predictors of female *A. burtoni* aggression (Renn et al., 2012). It is possible that magnocellular AVT cells mediate increased aggressiveness close to reproduction in *A. burtoni* females in a similar manner, but this deserves further research.

We also found that AVT immunoreactivity in gigantocellular POA cells was modulated by female reproductive state. In *A. burtoni* males, gigantocellular AVT expression correlated with display of male aggressive behaviors (Greenwood et al., 2008). In a weakly electric fish, more gigantocellular AVT cells were activated than magnocellular and parvocellular AVT cells in males exposed to a reproductive social stimulus compared to isolated males (Pouso, Goodson, & Silva, 2019).

In addition, the number of AVT-ir cells correlated with male reproductive behaviors. Similar to magnocellular cells, we found that gravid females had larger AVT-ir cell areas compared to brooding females. However, when separated by brooding stage, we found that late-stage brooding females had larger gigantocellular AVT cells than mid-brooding females and that cell size positively correlated with the number of days brooding. In a monogamous biparental cichlid, *Neolamprologus caudopunctatus*, females had higher whole brain AVT levels than males measured via HPLC, AVT levels were highest in fish that were defending their nest, and AVT levels correlated with the amount of the nest maintenance behaviors (Cunha-Saraiva et al., 2019). In addition, large, parental male half-spotted gobies had larger gigantocellular POA cells than males during other seasons (Maruska et al., 2007), so it is possible that gigantocellular AVT cells may have a role in parental behaviors in fishes. In contrast, administration of a vasotocin V1a receptor antagonist increased parental behaviors in *Amphiprion ocellaris* (DeAngelis, Gogola, Dodd, & Rhodes, 2017). Post-spawn medaka females have more nonapeptide POA cells than prespawn females (Ohya & Hayashi, 2006), but there was cross-reactivity of their vasotocin antibody with isotocin, and they quantified the whole POA, not specific cell types. Nevertheless, the authors suggest the decrease in nonapeptide positive cells is due to the abrupt release of AVT into circulation at spawning. And in the Hawaiian sergeant fish *Abudefduf abdominalis*, both males and females had more AVT-ir gigantocellular cells during peak spawning times compared to other seasons (Maruska, 2009). Similarly, our data could support a role of gigantocellular AVT cells in female spawning, as gigantocellular cell size was largest in ovulated, ready-to-spawn females and cell size increased throughout the brooding cycle. This could suggest that AVT peptide stores are high right before spawning, get released at spawning, and gradually replenish during mouthbrooding and recovery phases.

In the ventral hypothalamic group, brooding females had larger *avt* cells than gravid females. We also observed that males had fewer *avt*-expressing cells in the ventral hypothalamus than females. This group of AVT cells comes from a different embryonic origin than POA AVT cells and could have different regulatory mechanisms (Kagawa et al., 2016). In medaka, AVT expression was similar between males and females during development, but by adulthood, this group is completely absent in females (Kawabata, Hiraki, Takeuchi, & Okubo, 2012). This led the authors to suggest that these cells were involved in a male-biased or male-typical reproductive or aggressive behavior system. However, our data suggest the opposite. Due to their location and larger cell size in brooding females than ovulated females, we hypothesize that these cells are involved in mouthbrooding behaviors in *A. burtoni*. This could be related to functions supporting natural changes in feeding or parental care behaviors. For example, this population of *avt* cells is in close proximity to cells expressing many feeding-related peptides in *A. burtoni* (Porter et al., 2017). In goldfish, intracerebroventricular injections of AVT have an anorexigenic effect, with fish decreasing their cumulative food intake in a dose-dependent response (Araishi, Watanabe, Yamazaki, Nakamachi, & Matsuda, 2019). Similarly, central mesotocin

administration in chicks, but not peripheral administration, inhibits feeding behaviors (Masunari, Cline, Khan, & Tachibana, 2016), and AVT modulates NPY-induced food intake (Kuenzel, Hancock, Nagarajan, Aman, & Kang, 2016). Perhaps this population of *avt* cells in *A. burtoni* plays a role in inhibiting food intake during mouthbrooding, and future studies are needed to examine how the AVT system interacts with orexigenic and anorexigenic neuropeptides in this region.

4.3 | Use of various methods for examining the AVT system in fishes

Interestingly, we found that AVT-ir cells were only located in the preoptic area in *A. burtoni*, but *avt*-expressing cells were also located in the ventral hypothalamus and lateral diencephalon near PGa. We also found that *avt* cells were more abundant and larger than AVT-ir cells in the preoptic area. A similar phenomenon was detected in the blenniid fish *Salaria pavo*, with riboprobes producing much denser staining than IHC (Grober et al., 2002). This difference in peptide and mRNA staining is thought to be reflective of the large amount of *avt* transcripts present in these cells. While our double labels for AVT peptide and mRNA indicated that all AVT peptide containing cells had *avt*, there were many mRNA-expressing cells in the preoptic area that were not immunoreactive for AVT. One possibility is that our ISH probe was cross-reacting with isotocin. However, sequencing of the transcripts suggests this is not the case. Instead, it is possible that *avt* is not translated into protein in all of these cells or that protein is being made and quickly released or shuttled down axons, such that levels of AVT peptide in these cells is below the level of detection for IHC.

We quantified both the number and size of *avt*/AVT neurons. However, there is not always a straightforward relationship between somata size, cell number, mRNA levels, and protein levels within individual neurons. Overall, we used cell number as a proxy for the *possible* amount of avt/AVT that is produced, stored, and/or released. More neurons with *avt* transcripts or AVT peptide reflect more *possible* AVT signaling on a broader level. In contrast, somata size reflects *avt*/AVT signaling within an individual neuron. An increase in cell size could be due to an increase in peptide production and release or due to storage and reduced peptide release, but it is not possible to distinguish between these possibilities based on staining alone. In *A. burtoni*, it was proposed that changes in cell size, but not cell number, allow for quicker structural plasticity either induced by or required for the rapid phenotypic changes associated with male social status transitions and female mouthbrooding (Maruska, 2014; Maruska & Fernald, 2013; Porter et al., 2017). Future studies using microdialysis and quantitative analytic techniques (e.g., HPLC) are needed to accurately determine peptide concentration.

Despite no AVT-ir or *avt* cells in the Vs and Dm, *avt* transcripts were amplified via qPCR. It is possible that mRNA could be packaged and sent to projections where it is locally translated into AVT peptide, however, we did not observe any *avt* staining in what appeared to be

fibers in these regions. Despite using a genomic DNA eliminator column, it is also possible that this very low level of detection could be from genomic DNA contamination. It is important to note that although *avt* was detected in these regions, its expression was very low and only amplified in approximately half of the samples, raising questions about whether these low measured levels have any biological significance. Almost no AVT-ir fibers were seen in Dm and only few scattered fibers occurred in Vs, further suggesting any AVT input to these regions is minimal.

Genomic toolkits are rapidly expanding and with it come a variety of techniques for describing and localizing target gene and protein expression in the brain. In addition to IHC and ISH, *avt* distribution was examined using transgenic medaka carrying GFP in *avt* neurons (Kagawa et al., 2016; Ohya & Hayashi, 2006). These studies also corroborate the restricted distribution of AVT neurons in the POA and hypothalamus characteristic of most teleosts. In addition, HPLC was used to quantify AVT peptide abundance in brain regions and in circulation (Soares et al., 2017). With the rapid expansion and ever-improving techniques available, more studies are needed that compare methods and visualization techniques to gain a more complete and accurate understanding of biological significance.

With the advancement of molecular and analytical techniques, quantifying whole brain levels of AVT is now obsolete in most cases. Parvocellular, magnocellular, and gigantocellular AVT cells likely have different and sometimes contrasting functions across fishes. As demonstrated here, even measuring whole POA *avt* expression, independent of cell type and region, often does not reveal differences, but examining each cell type individually does. Future work on the AVT system in teleosts should be done with high neuroanatomical resolution and adequate controls to better understand the cell type-specific functions in this largest and most diverse group of vertebrates.

One final consideration for studies on the AVT system in fishes revolves around the use of wild-caught and lab-reared animals. Our laboratory-bred stock is descendants of *A. burtoni* caught in Lake Tanganyika in the 1970s. While some effort has been made to occasionally introduce new wild-caught animals to the laboratory stock, it is still likely and possible that some genetic drift and inbreeding has occurred. For example, some maternal behaviors differ between lab-reared and wild-caught females, with laboratory-reared females displaying higher rates of filial cannibalism and wild-caught females displaying more maternal care (Renn et al., 2009). While differences in behaviors occur, it is unlikely, however, that well-conserved neuropeptide systems, like AVT, have drastically diverged over the past ~50 years. Nonetheless, more well-controlled studies are needed on wild-caught animals to determine if and how neural circuitry governing social behaviors changes in laboratory-reared animals.

5 | CONCLUSIONS

Across fishes, cell size and cell number are often used as a proxy for the abundance of AVT peptide or mRNA. It is quite evident from numerous studies that there is a large species-dependent role of AVT, but several general themes have emerged. The results presented here provide complementary studies to those in male *A. burtoni*, and together, form a more complete picture on the role of AVT in complex social behaviors in both sexes. By incorporating our data in females, we propose the following updates to the model presented by Greenwood et al. (2008) and Loveland and Fernald (2017). Across teleosts, parvocellular AVT cells are involved in subordinate behaviors, particularly in male fishes. Magnocellular AVT cells appear to be important for display of aggressive behaviors and interact with neural circuits mediating aggression and territoriality in both male and female fishes (Larson et al., 2006). Based on our data, and that from gobies and a biparental cichlid (Cunha-Saraiva et al., 2019; Maruska et al., 2007), we hypothesize that gigantocellular AVT cells may be involved in display of parental care behavior in both sexes. And for the first time, ventral hypothalamic AVT cells can be included in this model as having a role in female mouthbrooding, which involves both parental care and modulation of food intake. Together, this updated model and the results presented here provide a new framework for investigating the behavioral roles of AVT subgroups in social and parental behaviors, especially in female fishes.

CONFLICT OF INTEREST
The authors declare no conflict of interest.

AUTHOR CONTRIBUTIONS
All authors had full access to all the data, take responsibility for the integrity of the data analysis, and approved the final article. Designed experiments: **Julie M. Butler** and **Karen P. Maruska**. Performed experiments, collected, and analyzed data: **Julie M. Butler** and **Chase M. Anselmo**. Wrote and edited the article: **Julie M. Butler**, **Chase M. Anselmo**, and **Karen P. Maruska**. Provided funding, equipment, reagents, and supplies: **Karen P. Maruska**.

PEER REVIEW
The peer review history for this article is available at https://publons.com/publon/10.1002/cne.24995.

DATA AVAILABILITY STATEMENT
All data will be made available upon reasonable request.

ORCID
Julie M. Butler https://orcid.org/0000-0002-7400-8780
Karen P. Maruska https://orcid.org/0000-0003-2425-872X

REFERENCES

Abercrombie, M. (1946). Estimation of nuclear population from microtome sections. *The Anatomical Record*, 94(2), 239–247.

Acher, R., & Chauvet, J. (1995). The neurohypophysial endocrine regulatory cascade: Precursors, mediators, receptors, and effectors. *Frontiers in Neuroendocrinology*, 16(3), 237–289.

Araishi, K., Watanabe, K., Yamazaki, T., Nakamachi, T., & Matsuda, K. (2019). Intracerebroventricular administration of arginine vasotocin (AVT) induces anorexigenesis and anxiety-like behavior in goldfish. *Peptides*, 119, 170118.

Boyd, S. K. (1994). Gonadal steroid modulation of vasotocin concentrations in the bullfrog brain. *Neuroendocrinology*, 60(2), 150–156.

Butler, J. M., & Maruska, K. P. (2016). The mechanosensory lateral line system mediates activation of socially-relevant brain regions during territorial interactions [Original Research]. *Frontiers in Behavioral Neuroscience*, 10(93), 10. https://doi.org/10.3389/fnbeh.2016.00093

Butler, J. M., & Maruska, K. P. (2019). Expression of tachykinin3 and related reproductive markers in the brain of the African cichlid fish *Astatotilapia burtoni*. *Journal of Comparative Neurology*, 527(7), 1210–1227. https://doi.org/10.1002/cne.24622

Butler, J. M., Whitlow, S. M., Rogers, L. S., Putland, R. L., Mensinger, A. F., & Maruska, K. P. (2019). Reproductive state-dependent plasticity in the visual system of an African cichlid fish. *Hormones and Behavior*, 114, 104539. https://doi.org/10.1016/j.yhbeh.2019.06.003

Cunha-Saraiva, F., Balshine, S., Gozdowska, M., Kulczykowska, E., Wagner, R. H., & Schaedelin, F. C. (2019). Parental care and neuropeptide dynamics in a cichlid fish *Neolamprologus caudopunctatus*. *Hormones and Behavior*, 116, 104576.

DeAngelis, R., Gogola, J., Dodd, L., & Rhodes, J. S. (2017). Opposite effects of nonapeptide antagonists on paternal behavior in the teleost fish *Amphiprion ocellaris*. *Hormones and Behavior*, 90, 113–119.

Dewan, A., Maruska, K., & Tricas, T. (2008). Arginine vasotocin neuronal phenotypes among congeneric territorial and shoaling reef butterflyfishes: Species, sex and reproductive season comparisons. *Journal of Neuroendocrinology*, 20(12), 1382–1394.

Dewan, A. K., Ramey, M. L., & Tricas, T. C. (2011). Arginine vasotocin neuronal phenotypes, telencephalic fiber varicosities, and social behavior in butterflyfishes (Chaetodontidae): Potential similarities to birds and mammals. *Hormones and Behavior*, 59(1), 56–66.

Fernald, R. D. (1977). Quantitative behavioural observations of *Haplochromis burtoni* under semi-natural conditions. *Animal Behaviour*, 25(Pt 3), 643–653. https://doi.org/10.1016/0003-3472(77)90115-4

Fernald, R. D., & Hirata, N. R. (1977). Field study of *Haplochromis burtoni*: Quantitative behavioural observations. *Animal Behaviour*, 25(4), 964–975. https://doi.org/10.1016/0003-3472(77)90048-3

Fernald, R. D., & Shelton, L. C. (1985). The organization of the diencephalon and the pretectum in the cichlid fish, *Haplochromis burtoni*. *Journal of Comparative Neurology*, 238(2), 202–217. https://doi.org/10.1002/cne.902380207

Field, K. E., & Maruska, K. P. (2017). Context-dependent chemosensory signaling, aggression and neural activation patterns in gravid female African cichlid fish. *Journal of Experimental Biology*, 220(24), 4689–4702.

Foran, C. M., & Bass, A. H. (1998). Preoptic AVT immunoreactive neurons of a teleost fish with alternative reproductive tactics. *General and Comparative Endocrinology*, 111(3), 271–282.

Godwin, J., Sawby, R., Warner, R. R., Crews, D., & Grober, M. S. (2000). Hypothalamic arginine vasotocin mRNA abundance variation across sexes and with sex change in a coral reef fish. *Brain, Behavior and Evolution*, 55(2), 77–84.

Godwin, J., & Thompson, R. (2012). Nonapeptides and social behavior in fishes. *Hormones and Behavior*, 61(3), 230–238.

Goodson, J. L., & Bass, A. H. (2000). Vasotocin innervation and modulation of vocal-acoustic circuitry in the teleost *Porichthys notatus*. *Journal of Comparative Neurology*, 422(3), 363–379.

Goodson, J. L., Evans, A. K., & Bass, A. H. (2003). Putative isotocin distributions in sonic fish: Relation to vasotocin and vocal–acoustic circuitry. *Journal of Comparative Neurology*, 462(1), 1–14.

Goossens, N., Dierickx, K., & Vandesande, F. (1977). Immunocytochemical localization of vasotocin and isotocin in the preopticohypophysial neurosecretory system of teleosts. *General and Comparative Endocrinology*, 32(4), 371–375.

Gozdowska, M., Kleszczyńska, A., Sokołowska, E., & Kulczykowska, E. (2006). Arginine vasotocin (AVT) and isotocin (IT) in fish brain: Diurnal and seasonal variations. *Comparative Biochemistry and Physiology Part B: Biochemistry and Molecular Biology*, 143(3), 330–334.

Greenwood, A. K., Wark, A. R., Fernald, R. D., & Hofmann, H. A. (2008). Expression of arginine vasotocin in distinct preoptic regions is associated with dominant and subordinate behaviour in an African cichlid fish. *Proceedings of the Biological Sciences*, 275(1649), 2393–2402.

Grober, M. S., George, A. A., Watkins, K. K., Carneiro, L. A., & Oliveira, R. F. (2002). Forebrain AVT and courtship in a fish with male alternative reproductive tactics. *Brain Research Bulletin*, 57(3–4), 423–425.

Grone, B. P., & Maruska, K. P. (2015). A second corticotropin-releasing hormone gene (CRH2) is conserved across vertebrate classes and expressed in the hindbrain of a basal Neopterygian fish, the spotted gar (*Lepisosteus oculatus*). *Journal of Comparative Neurology*, 523(7), 1125–1143.

Kagawa, N. (2013). Social rank-dependent expression of arginine vasotocin in distinct preoptic regions in male *Oryzias latipes*. *Journal of Fish Biology*, 82(1), 354–363.

Kagawa, N., Honda, A., Zenno, A., Omoto, R., Imanaka, S., Takehana, Y., & Naruse, K. (2016). Arginine vasotocin neuronal development and its projection in the adult brain of the medaka. *Neuroscience Letters*, 613, 47–53.

Kalamarz-Kubiak, H., Gozdowska, M., Guellard, T., & Kulczykowska, E. (2017). How does oestradiol influence the AVT/IT system in female round gobies during different reproductive phases? *Biology Open*, 6(10), 1493–1501.

Kapsimali, M., Bourrat, F., & Vernier, P. (2001). Distribution of the orphan nuclear receptor Nurr1 in medaka (*Oryzias latipes*): Cues to the definition of homologous cell groups in the vertebrate brain. *Journal of Comparative Neurology*, 431(3), 276–292.

Kawabata, Y., Hiraki, T., Takeuchi, A., & Okubo, K. (2012). Sex differences in the expression of vasotocin/isotocin, gonadotropin-releasing hormone, and tyrosine and tryptophan hydroxylase family genes in the medaka brain. *Neuroscience*, 218, 65–77.

Kelly, A. M., & Goodson, J. L. (2014). Social functions of individual vasopressin–oxytocin cell groups in vertebrates: What do we really know? *Frontiers in Neuroendocrinology*, 35(4), 512–529.

Kuenzel, W. J., Hancock, M., Nagarajan, G., Aman, N. A., & Kang, S. W. (2016). Central effect of vasotocin 4 receptor (VT4R/V1aR) antagonists on the stress response and food intake in chicks given neuropeptide Y (NPY). *Neuroscience Letters*, 620, 57–61.

Larson, E. T., O'Malley, D. M., & Melloni, R. H., Jr. (2006). Aggression and vasotocin are associated with dominant–subordinate relationships in zebrafish. *Behavioural Brain Research*, 167(1), 94–102.

Loveland, J. L., & Fernald, R. D. (2017). Differential activation of vasotocin neurons in contexts that elicit aggression and courtship. *Behavioural Brain Research*, 317, 188–203.

Loveland, J. L., & Hu, C. K. (2018). Commentary: Arginine vasotocin preprohormone is expressed in surprising regions of the teleost forebrain. *Frontiers in Endocrinology*, 9(63). https://doi.org/10.3389/fendo.2018.00063

Maruska, K. P. (2009). Sex and temporal variations of the vasotocin neuronal system in the damselfish brain. *General and Comparative Endocrinology*, 160(2), 194–204.

Maruska, K. P. (2014). Social regulation of reproduction in male cichlid fishes. *General and Comparative Endocrinology*, *207*, 2–12.

Maruska, K. P., Butler, J. M., Anselmo, C. M., & Tandukar, G. (2020). Distributuon of aromatase in the brain of the African cichlid fish *Astatotilapia burtoni*: Aromatase expression, but not estrogen receptors, varies with female reproductive state. *Journal of Comparative Neurology*.

Maruska, K. P., Butler, J. M., Field, K. E., & Porter, D. T. (2017). Localization of glutamatergic, GABAergic, and cholinergic neurons in the brain of the African cichlid fish, *Astatotilapia burtoni*. *Journal of Comparative Neurology*, *525*, 610–638.

Maruska, K. P., & Fernald, R. D. (2010). Steroid receptor expression in the fish inner ear varies with sex, social status, and reproductive state. *BMC Neuroscience*, *11*(1), 1.

Maruska, K. P., & Fernald, R. D. (2013). Social regulation of male reproductive plasticity in an African cichlid fish. *Integrative and Comparative Biology*, *53*, 938–950.

Maruska, K. P., & Fernald, R. D. (2018). *Astatotilapia burtoni*: A model system for analyzing the neurobiology of behavior. *ACS Chemical Neuroscience*, *9*, 1951–1962. https://doi.org/10.1021/acschemneuro.7b00496

Maruska, K. P., Mizobe, M. H., & Tricas, T. C. (2007). Sex and seasonal covariation of arginine vasotocin (AVT) and gonadotropin-releasing hormone (GnRH) neurons in the brain of the halfspotted goby. *Comparative Biochemistry and Physiology Part A: Molecular & Integrative Physiology*, *147*(1), 129–144.

Masunari, K., Cline, M. A., Khan, S. I., & Tachibana, T. (2016). Feeding response following central administration of mesotocin and arginine-vasotocin receptor agonists in chicks (*Gallus gallus*). *Physiology & Behavior*, *153*, 149–154.

Miller, M. A., Urban, J. H., & Dorsa, D. M. (1989). Steroid dependency of vasopressin neurons in the bed nucleus of the stria terminalis by in situ hybridization. *Endocrinology*, *125*(5), 2335–2340.

Munchrath, L. A., & Hofmann, H. A. (2010). Distribution of sex steroid hormone receptors in the brain of an African cichlid fish, *Astatotilapia burtoni*. *Journal of Comparative Neurology*, *518*(16), 3302–3326.

O'Connell, L. A., Fontenot, M. R., & Hofmann, H. A. (2011). Characterization of the dopaminergic system in the brain of an African cichlid fish, *Astatotilapia burtoni*. *Journal of Comparative Neurology*, *519*(1), 75–92.

Ohya, T., & Hayashi, S. (2006). Vasotocin/isotocin-immunoreactive neurons in the medaka fish brain are sexually dimorphic and their numbers decrease after spawning in the female. *Zoological Science*, *23*(1), 23–29.

Olivereau, M., Moons, L., Olivereau, J., & Vandesande, F. (1988). Coexistence of corticotropin-releasing factor-like immunoreactivity and vasotocin in perikarya of the preoptic nucleus in the eel. *General and Comparative Endocrinology*, *70*(1), 41–48.

Porter, D. T., Roberts, D. A., & Maruska, K. P. (2017). Distribution and female reproductive state differences in orexigenic and anorexigenic neurons in the brain of the mouth brooding African cichlid fish, *Astatotilapia burtoni*. *Journal of Comparative Neurology*, *525*, 3126–3157.

Pouso, P., Goodson, J. L., & Silva, A. (2019). Preoptic area activation and vasotocin involvement in the reproductive behavior of a weakly pulse-type electric fish, *Brachyhypopomus gauderio*. *Frontiers in Integrative Neuroscience*, *13*, 37.

Ramallo, M. R., Grober, M., Cánepa, M. M., Morandini, L., & Pandolfi, M. (2012). Arginine-vasotocin expression and participation in reproduction and social behavior in males of the cichlid fish *Cichlasoma dimerus*. *General and Comparative Endocrinology*, *179*(2), 221–231.

Renn, S. C., Fraser, E. J., Aubin-Horth, N., Trainor, B. C., & Hofmann, H. A. (2012). Females of an African cichlid fish display male-typical social dominance behavior and elevated androgens in the absence of males. *Hormones and Behavior*, *61*(4), 496–503.

Renn, S. C., Carleton, J. B., Magee, H., Nguyen, M. L. T., & Tanner, A. C. (2009). Maternal care and altered social phenotype in a recently collected stock of Astatotilapia burtoni cichlid fish. *Integrative and Comparative Biology*, *49*(6), 660–673.

Rodríguez-Illamola, A., Patiño, M. A. L., Soengas, J. L., Ceinos, R. M., & Míguez, J. M. (2011). Diurnal rhythms in hypothalamic/pituitary AVT synthesis and secretion in rainbow trout: Evidence for a circadian regulation. *General and Comparative Endocrinology*, *170*(3), 541–549.

Rodriguez-Santiago, M., Nguyen, J., Winton, L. S., Weitekamp, C. A., & Hofmann, H. A. (2017). Arginine vasotocin preprohormone is expressed in surprising regions of the teleost forebrain. *Frontiers in Endocrinology*, *8*(195). https://doi.org/10.3389/fendo.2017.00195

Saito, D., Komatsuda, M., & Urano, A. (2004). Functional organization of preoptic vasotocin and isotocin neurons in the brain of rainbow trout: Central and neurohypophysial projections of single neurons. *Neuroscience*, *124*(4), 973–984. https://doi.org/10.1016/j.neuroscience.2003.12.038

Semsar, K., & Godwin, J. (2003). Social influences on the arginine vasotocin system are independent of gonads in a sex-changing fish. *Journal of Neuroscience*, *23*(10), 4386–4393.

Semsar, K., Kandel, F. L., & Godwin, J. (2001). Manipulations of the AVT system shift social status and related courtship and aggressive behavior in the bluehead wrasse. *Hormones and Behavior*, *40*(1), 21–31.

Sladek, C. D., & Somponpun, S. J. (2008). Estrogen receptors: Their roles in regulation of vasopressin release for maintenance of fluid and electrolyte homeostasis. *Frontiers in Neuroendocrinology*, *29*(1), 114–127.

Soares, M. C., Cardoso, S. C., Mazzei, R., Andre, G. I., Morais, M., Gozdowska, M., … Kulczykowska, E. (2017). Region specific changes in nonapeptide levels during client fish interactions with allopatric and sympatric cleaner fish. *PLoS One*, *12*(7), e0180290.

van den Dungen, H. M., Buijs, R. M., Pool, C. W., & Terlou, M. (1982). The distribution of vasotocin and isotocin in the brain of the rainbow trout. *Journal of Comparative Neurology*, *212*(2), 146–157. https://doi.org/10.1002/cne.902120205

Zhao, S., & Fernald, R. D. (2005). Comprehensive algorithm for quantitative real-time polymerase chain reaction. *Journal of Computational Biology*, *12*(8), 1047–1064.